Strain-Tuned Incompatible Magnetic Exchange-Interaction in La_2NiO_4

I. Biało,[1,2,*] L. Martinelli,[1] G. De Luca,[3] P. Worm,[4] A. Drewanowski,[1] S. Jöhr,[1] J. Choi,[5] M. Garcia-Fernandez,[5] S. Agrestini,[5] Ke-Jin Zhou,[5] K. Kummer,[6] N. B. Brookes,[6] L. Guo,[7] A. Edgeton,[7] C. B. Eom,[7] J. M. Tomczak,[8,4] K. Held,[4] M. Gibert,[4] Qisi Wang,[9,1,†] and J. Chang[1]

[1] *Physik-Institut, Universität Zürich, Winterthurerstrasse 190, CH-8057 Zürich, Switzerland*
[2] *AGH University of Krakow, Faculty of Physics and Applied Computer Science, 30-059 Krakow, Poland*
[3] *Institut de Ciència de Materials de Barcelona (ICMAB-CSIC), 08193 Bellaterra (Barcelona), Spain*
[4] *Institute of Solid State Physics, Vienna University of Technology, A-1040 Vienna, Austria*
[5] *Diamond Light Source, Harwell Campus, Didcot, Oxfordshire OX11 0DE, United Kingdom*
[6] *ESRF, The European Synchrotron, 71 Avenue des Martyrs, CS40220, 38043 Grenoble Cedex 9, France*
[7] *Department of Materials Science and Engineering, University of Wisconsin-Madison, Madison, 53706, Wisconsin, USA*
[8] *Department of Physics, King's College London, Strand, London WC2R 2LS, United Kingdom*
[9] *Department of Physics, The Chinese University of Hong Kong, Shatin, Hong Kong, China*

(Dated: March 22, 2024)

Keywords: Magnetic Frustration; Resonant Inelastic X-ray Scattering; Exchange Interactions

Magnetic frustration is a route for novel ground states, including spin liquids and spin ices. Such frustration can be introduced through either lattice geometry or incompatible exchange interactions. Here, we find that epitaxial strain is an effective tool for tuning antiferromagnetic (AF) exchange interactions in square-lattice system. By studying the magnon excitations in La_2NiO_4 films using resonant inelastic x-ray scattering (RIXS) we show that the magnon dispersion peaks at the AF zone boundary, at energies that dependent on the lattice ~~properties~~ of the film's substrate. This indicates the presence of AF nearest neighbor (NN) and AF next-nearest neighbor (NNN) spin interaction that can be tuned by epitaxial strain. Using first principles simulations and an effective spin model, we demonstrate that the AF-NNN coupling is a consequence of the two-orbital nature of La_2NiO_4. By exploring La_2NiO_4 films grown on different substrates, we illustrate that compressive epitaxial strain enhances this coupling and, as a result, increases the level of incompatibility between exchange interactions within a model square-lattice system.

Introduction

The square-lattice Heisenberg model is the subject of intense numerical and experimental investigations. In spin-1/2 systems—such as cuprates [1] and copper deuteroformate tetradeurate (CFTD) [2]—higher-order exchange interactions are inferred from observations of magnon dispersions along the magnetic zone boundary [3, 4]. While a detailed magnon characterization is useful to understand quantum-fluctuation effects [5], exchange incompatibility is typically avoided in these systems. Indeed, the antiferromagnetic (AF) nearest-neighbor (NN) exchange interaction ($J_1 > 0$) and the ferromagnetic next-nearest-neighbour (NNN) interaction ($J_2 < 0$) in these systems stabilize ~~a~~ the classical AF Néel order. Instead, magnetic exchange incompatibility requires both $J_1 > 0$ and $J_2 > 0$. This regime of the J_1-J_2 model is the subject of extensive computational investigations for both spin $S = 1/2$ [6–10] and $S = 1$ [11, 12] systems. In a narrow range near $J_2/J_1 \sim 1/2$, magnetic frustration is found to dominate, and exotic quantum phases such as the spin-liquid state [13] are predicted. Several calculations show that the Néel order is destroyed there and the ground state has a valence-bond character [13–15], although its exact nature is still the subject of debate [8, 16]. However, only very few square-lattice systems exhibit substantial magnetic frustration [17, 18], and even fewer display tunable magnetic interactions [19]. As a result, approaching the interesting parameter regime in real materials remains an ongoing issue.

In this article, we provide a high resolution resonant inelastic x-ray scattering (RIXS) study of magnetic excitations in epitaxial thin films of the canonical $S = 1$ system La_2NiO_4, grown on different substrates. We discover a marked, upward dispersion along the AF zone-boundary $(1/2, 0) \rightarrow (1/4, 1/4)$, which reveals the presence of ~~strong,~~ AF-NNN interactions that partly frustrate the NN ones. By employing *ab initio* calculations, we demonstrate that these results can only be explained by including the multi-orbital nature of $3d^8$-Ni systems. More interestingly, we observe a correlation between the relative strength of the magnetic interactions and the strain applied onto the films. Our results demonstrate that 214-type nickelates are a promising class of materials for the study of the AF~~,~~ square-lattice Heisenberg model. Moreover, the use of thin films provides a clear route to tune the magnetic frustration and explore so far inaccessible regions of the magnetic phase diagram.

* izabela.bialo@uzh.ch
† qwang@cuhk.edu.hk

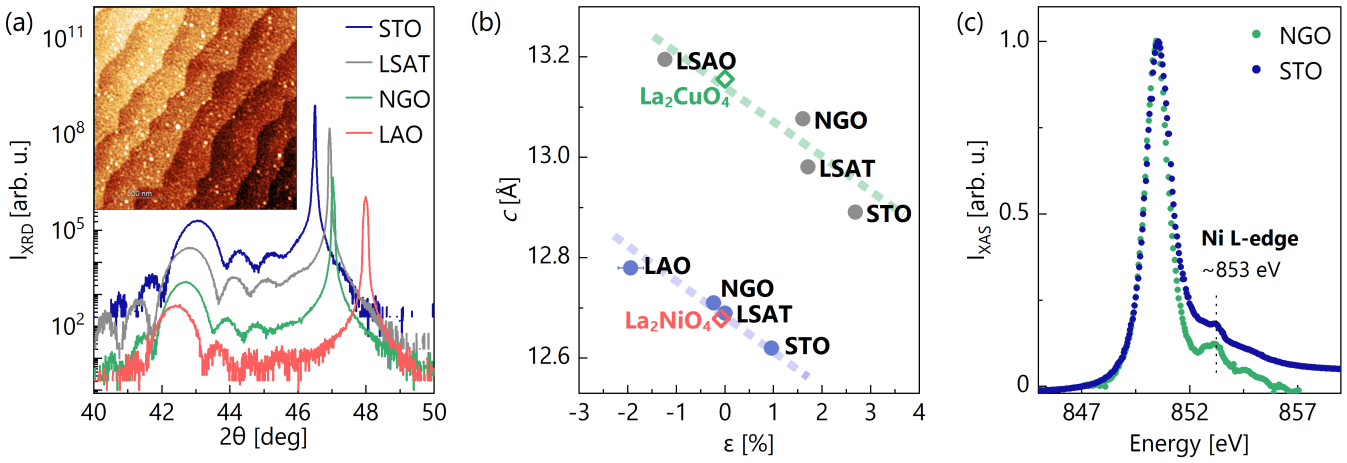

FIG. 1. **Characterization measurements on thin films of La_2NiO_4.** (a) X-ray diffraction (at 300 K) probing the $(0, 0, \ell)$ direction of 12 nm thin films of La_2NiO_4 on substrates as indicated. The inset represents the atomic force microscopy image showing the step-like morphology of the films (here for the NGO substrate). The color scale corresponds to ~~the~~ film thickness. (b) c-axis lattice parameter versus in-plane epitaxial strain (at 300 K) calculated for LNO (purple dots) and La_2CuO_4 [20] (gray dots) films grown on different substrates as a relative change of in-plane parameters in reference to bulk (diamonds) with $a = 3.868$ Å and $c = 12.679$ Å for an isomorphic La_2NiO_4 structure [21] and $a = 3.803$ Å and $c = 13.156$ Å for La_2CuO_4 [22]. (c) X-ray absorption spectra around the Ni L-edge. The dominant peak corresponds to the La M-edge. (b,c) Dashed lines are guides to the eye.

Results

Our thin films of La_2NiO_4 (LNO) on $SrTiO_3$ (STO), $LaAlO_3$ (LAO), $(LaAlO_3)_{0.3}(Sr_2TaAlO_6)_{0.7}$ (LSAT) and $NdGaO_3$ (NGO) substrates are characterized by atomic force microscopy (AFM), x-ray diffraction (XRD), and x-ray absorption spectroscopy (XAS) – see Fig. 1. The AFM images display a ~~step-like~~ steplike morphology indicating an excellent layer-by-layer growth. Diffraction patterns probing the $(0, 0, \ell)$ reciprocal direction demonstrate good single crystallinity and allow us to extract the c-axis lattice parameters of the films. The epitaxial strain applied by the substrates is supported by the film c-axis and in-plane lattice-parameter dependence (Fig. 1b). ~~The~~ XAS spectra recorded on the LNO/STO and LNO/NGO, shown in Fig. 1c., are consistent with ~~what is observed~~ observations on related nickelates [23–26]. The Ni $L-$edge features on the tail of the La M -edge.

The RIXS spectra of LNO films were measured at the Ni L_3 edge (853 eV). These spectra exhibit key RIXS excitations, including high-energy dd-excitations (at approximately 0.5-3 eV), an elastic scattering contribution at 0 eV, as well as phonon and magnon excitations in between. The dd-excitations have a multi-peak structure, qualitatively similar to other $3d^8$ systems, such as NiO [23–25, 27]. As shown in Figs. 2a, the relative intensities of the peaks are different in the three samples, due to the different crystal-fields acting on the Ni atoms (see Fig. S1 in Supplementary Information). The subtraction of the elastic peak clearly highlights the presence of multiple low-energy features; see Figs. 2b,c.

~~The energy resolution of RIXS [28] has been constantly continuously improving in recent years. As a result, higher-order magnetic exchange interactions have been measured with exquisite precision [29] and, more recently, momentum-dependent electron-phonon couplings [30] have been extracted.~~ To extract the dispersion of magnetic excitations, we assumed a two-mode model with the addition of a high-energy continuum "background" (Fig. 2b,c). Each of these components is represented by a Gaussian profile. This provides an effective fitting model of excitations for all measured film systems and momenta. Our interpretation of the proposed model is based on the hypothesis that the lower-energy mode (~40 meV) stems from an optical phonon, while the higher-energy mode (strongly dispersing between 60 and 120 meV) is a magnon. This assignment is supported by previous neutron scattering measurements that identified the phonon part via an out-of-plane oxygen buckling mode [31, 32]. The interpretation of the higher-energy mode as a magnon is consistent with earlier RIXS [33] and neutron studies [34] of bulk La_2NiO_4. The resulting magnon dispersions are shown in Fig. 3.

Due to lower energy resolution, the previous RIXS study [33] did not resolve any phonon excitations. The unresolved phonon excitation implied that the phonon and magnon spectral weights were merged. This, in turn influences the extraction of the magnon dispersion. Having access, in this work, to a higher energy resolution, we can distinguish between the nearly momentum-independent phonon mode and the dispersive magnon branch along the three measured high-symmetry directions. In all the film systems explored, the magnon energy reaches its maximum at the

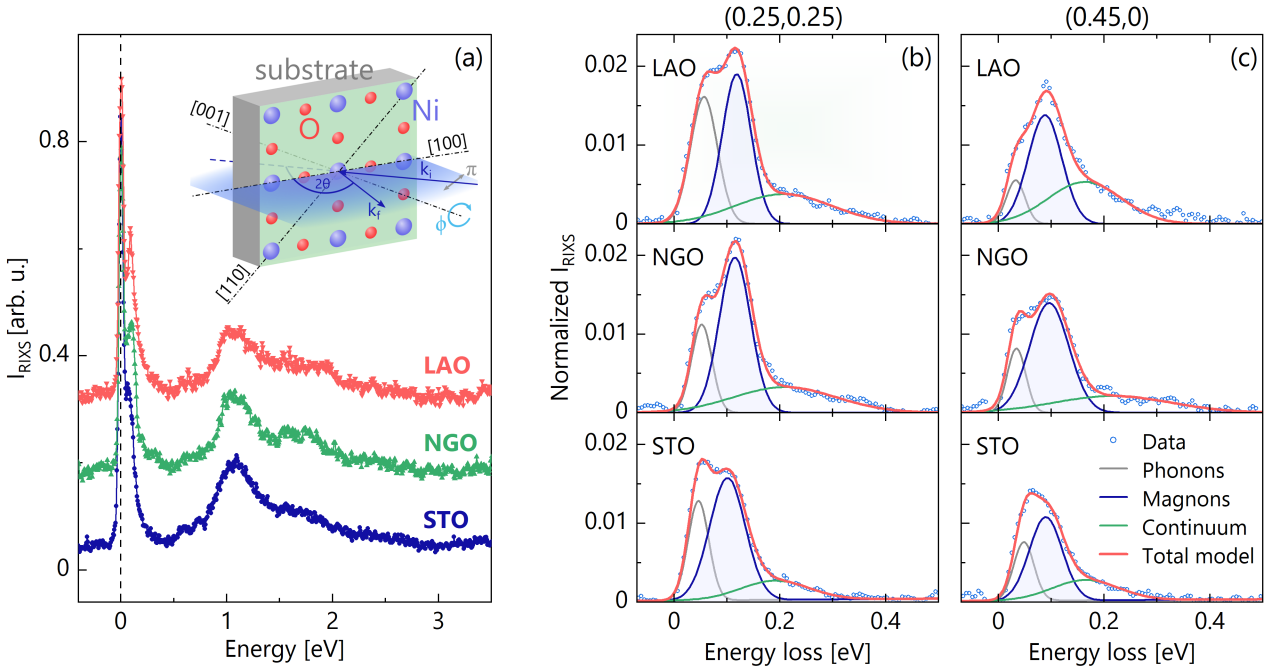

FIG. 2. **Resonant inelastic x-ray scattering spectra of LNO.** (a) Raw spectra recorded in LNO films with substrates as indicated. (a,inset) Schematics of the photon-in-photon-out RIXS geometry with horizontally polarized light (π) and azimuthal sample rotation angle ϕ. (b,c) Low-energy part of the RIXS spectra with momentum transfer and film substrates indicated. The solid red line indicates a three-component fit (see text) with phonon, magnon (shaded), and multi-magnon (continuum) contributions. The elastic scattering channel is subtracted in (b,c).

AF zone boundary, at the Σ point $(1/4, 1/4)$, referred to as E_Σ, while it displays a local minimum at the X point $(1/2, 0)$, referred to as E_X. This evidently anisotropic shape of magnon dispersion was not reported in earlier studies [33, 34], except for a recent inelastic neutron scattering experiment [35]. Furthermore, the energy E_Σ is different for all three substrates. In particular, it increases as a function of compressive strain, with an enhancement of 18 ± 4 meV ($\sim 20\%$) from LNO/STO to LNO/LAO.

Discussion

By resolving both the phonon and magnon modes, we find that all samples exhibit a substantial dispersion of magnetic excitations along the AF zone boundary. This ~~observation lifts the inconsistency between previous magnon studies of La_2NiO_4~~ directly implies~~ing~~ the presence of higher-order effective magnetic exchange interactions. In La_2CuO_4 and related Mott insulating cuprates, the zone boundary dispersion has been interpreted in terms of a positive ring-exchange interaction that emerges naturally from a *single-orbital* Hubbard model [20, 36, 37]. There is, however, an important difference between the zone-boundary dispersion of La_2CuO_4 and La_2NiO_4: in contrast to La_2CuO_4, the zone boundary dispersion of La_2NiO_4 has its maximum at the AF zone boundary Σ point rather than at the X point. As such, the magnon dispersion of La_2NiO_4 ~~cannot be described from~~ is (as could be expected) inconsistent with a single-band Hubbard model ~~—at least not~~ in the strong coupling limit (where the projection onto a Heisenberg spin Hamiltonian is viable).

As a first step, we parameterize the magnon dispersion of LNO using a phenomenological spin-wave model that includes effective NN and NNN exchange interactions, respectively J_1 and J_2 (Fig. 3), plus an easy-plane anisotropy K, already reported by previous measurements [34, 35]. As a starting point, we employ the AF structure of the bulk La_2NiO_4 determined by neutron diffraction [38–40], with the spin direction parallel to the crystallographic a-axis. The model is solved in a linear spin-wave (large-S) limit, and the calculated dispersion is fitted to the measured one (see Methods). Fitting the experimental ("exp") data yields an effective NN exchange interaction $J_1^{\rm exp} \sim 30$ meV consistent with previous neutron and RIXS results [33, 41]. Due to the demonstrated finite zone-boundary dispersion, our spin-wave model fitting also yields a moderate NNN exchange interaction $J_2^{\rm exp}$. Importantly, $J_2^{\rm exp}$ is *positive* and enhanced by compressive strain [3, 4]. In what follows, we wish to extract the frustration parameter $\mathcal{G} = J_2^{\rm exp}/J_1^{\rm exp}$ with the highest precision. Within our spin-wave model, $E_X = 4SZ_c(J_1 - 2J_2)$ and $E_\Sigma = 4SZ_c(J_1 - J_2)$, where Z_c is the quantum renormalization factor for spin-wave energies, which is taken as $Z_c = 1.09$ [42]. This gives $\mathcal{G}^{-1} = 1 + E_\Sigma/(E_\Sigma - E_X)$. The frustration parameter $\mathcal{G}$

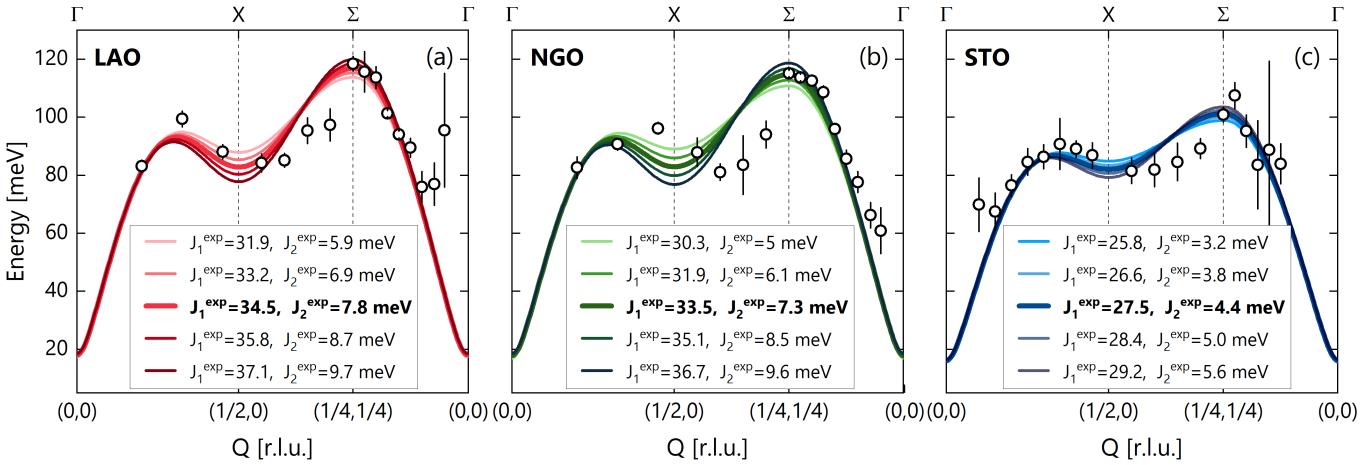

FIG. 3. **Magnon dispersion of La_2NiO_4 films.** (a-c) Magnon excitation energies (open dots) along high symmetry directions for La_2NiO_4 on substrates as indicated. Solid lines represent the same spin wave model (see text) evaluated for different exchange parameters within the confidence intervals of the fitted parameters. The curves corresponding to the best-fit values (marked ~~with~~ in bold in the legend) are reported as thicker lines. The middle segment, $X \to \Sigma$, is part of the AF zone-boundary. The error bars are determined from the fitting uncertainty.

is thus derived directly from the experimental data, with high precision (E_Σ and E_X are extracted with error lower than 5 meV) and plotted as a function of the c lattice parameter in Fig. 4 (see also Table S1 in Supplementary Information). Due to the Poisson effect, the c lattice parameter undergoes a proportional shrinkage when the in-plane parameters expand. Our XRD measurements confirm this relationship (Fig. 1b), indicating that the c-axis lattice parameter can serve as ~~a direct~~ an indirect probe of the in-plane strain. Therefore, our findings demonstrate a nearly linear correlation between magnetic frustrations and epitaxial strain.

We stress that, for interaction strengths and hoppings that are realistic for cuprates and nickelates, $J_2 > 0$ is hard to reconcile with a single-band Hubbard model. A positive J_2 implies an effective AF NNN exchange interaction, at odds with what is observed in cuprates [4, 36] and d^9 infinite-layer nickelates [43, 44]. Both systems have indeed been successfully described using a single d-orbital framework [3, 4, 45, 46]. Therefore, we argue that the magnon zone boundary dispersion in LNO signals physics beyond the single-orbital Hubbard model. We propose that the multi-orbital ($d_{x^2-y^2}$, d_{z^2}) nature of nickelates [47–49] must be explicitly considered. Already in La_2CuO_4, due to the short apical oxygen distance, a small but significant orbital hybridization between d_{z^2} and $d_{x^2-y^2}$ has been reported [50]. In La_2NiO_4 the apical oxygen distance is even shorter, as exemplified by the reduced c lattice parameter (see Fig. 1b), and hence an even more pronounced hybridization is expected.

To rationalize the trend in the exchange interactions obtained from our spin-wave fits, we derive a two-orbital low-energy model for La_2NiO_4 on different substrates from first principles (see the Method section). For the Ni d_{z^2} and $d_{x^2-y^2}$ orbitals (labeled "α" and "β"), we compute the (next) nearest-neighbor hopping parameters $t^{(\prime)}$, the crystal field splitting Δ_{eg}, local Coulomb (Hubbard) interaction U and Hund's exchange J_H using experimental lattice constants from Table I. Noteworthy[51], the hopping parameters and Coulomb interactions, listed in Table I, hardly change under varying in-plane compression. This is different from calculations for the cuprate family, see Ref. 20, and agrees with our experiments, which show substantially smaller changes in the magnon spectrum than for the cuprates. What is most affected by strain in Table I is the crystal-field splitting Δ_{eg} by which the Ni $d_{x^2-y^2}$ orbital is higher in energy than the d_{z^2} orbital. When going from the STO to the LAO substrate, in-plane strain pushes the $d_{x^2-y^2}$ orbital further up in energy, as it is pointing towards the now closer in-plane oxygen sites that are charged negatively.

This crystal-field splitting Δ_{eg} enters the calculated ("cal") two-orbital superexchange as follows:

$$J_1^{\rm cal} = \frac{t_{\alpha\beta}^2}{U + J_H - \Delta_{eg}} + \frac{t_{\alpha\beta}^2}{U + J_H + \Delta_{eg}} + \frac{t_{\alpha\alpha}^2 + t_{\beta\beta}^2}{U + J_H}\,, \tag{1}$$

where we extend the formula of Ref. 52 to finite Δ_{eg} (see Supplementary Information). As Δ_{eg} appears once with a plus and once with a minus sign in the denominator, the crystal-field splitting enters $J_1^{\rm cal}$ in a higher-than-linear order.

The magnetic exchange couplings $J_1^{\rm cal}$ determined by Eq. (1) are displayed in Table I. They show the same qualitative tendency as in our experiment, i.e., an increase of both $J_1^{\rm exp}$ (see Fig. 3) and $J_1^{\rm cal}$ with compressive strain. Quantitatively, the *ab initio* calculated $J_1^{\rm cal}$ is however notably too large. This has two major origins: (i) The cRPA interactions are, here, taken at zero frequency $U = U(\omega = 0)$. Additional renormalizations from

System	a [Å]	c [Å]	Δ_{eg} [eV]	$t_{\alpha\alpha}$ [eV]	$t_{\beta\beta}$ [eV]	$t_{\alpha\beta}$ [eV]	$t'_{\alpha\alpha}$ [meV]	$t'_{\beta\beta}$ [meV]	$U_{\alpha\alpha}$ [eV]	$U_{\beta\beta}$ [eV]	$U_{\alpha\beta}$ [eV]	J_H [eV]	$J_1^{\rm cal}$ [meV]	$J_2^{\rm cal}$ [meV]	$J_1^{\rm cal,corr}$ [meV]
La_2NiO_4	3.890	12.55	0.48	-0.070	-0.403	-0.161	-8.6	74.9	3.06	3.15	1.97	0.52	60.7	1.57	51.0
LNO/STO	3.905	12.62	0.48	-0.067	-0.395	-0.156	-8.3	74.5	3.01	3.14	1.94	0.52	59.5	1.56	49.7
LNO/LSAT	3.868	12.69	0.55	-0.065	-0.410	-0.156	-7.4	76.3	3.00	3.11	1.92	0.51	62.2	1.65	51.8
LNO/NGO	3.859	12.71	0.58	-0.064	-0.414	-0.155	-7.1	76.7	3.03	3.16	1.97	0.51	62.3	1.65	51.9
LNO/LAO	3.793	12.78	0.74	-0.060	-0.447	-0.156	-5.5	80.5	3.02	3.08	1.93	0.50	71.6	1.83	56.8

TABLE I. Crystal field splitting Δ_{eg}, (next-)nearest neighbor hopping $t_{ij}^{(\prime)}$ between i-th and j-th Ni orbitals (α and β here denote the z^2 and x^2-y^2 orbital, respectively), the inter- and intra-orbital Coulomb interaction U_{ij}, and Hund's exchange J_H between the two orbital as calculated by DFT and cRPA with the in-plane lattice constant a of the three substrates; note that $t'_{\alpha\beta}=0$ by symmetry. From these *ab initio* calculated parameters the spin couplings J_1 and J_2 are calculated from super-exchange (second order perturbation theory), i.e., from Eq. (1) with t and t', respectively. Estimating higher order terms using a one-orbital analogy, yields the reduced $J_1^{\rm cal,corr}$ couplings – see text. The bulk lattice parameters refer to the low temperature tetragonal polymorph of La_2NiO_4, after Ref. 35.

the frequency dependence $U(\omega)$ [53] are often mimicked through an empirical enhancement of U. Increasing U, we could easily obtain quantitative agreement with the experimental J_1, but at the cost of a free fit parameter and most likely only an accidental agreement. (ii) Eq. (1) only includes terms to second-order perturbation theory in t. For the one-band Hubbard model, higher-order processes have been calculated and yield a correction from $J_1 = 4t^2/U$ to a reduced $J_1 = 4(t^2/U - 16t^4/U^3)$ [45, 54]. Higher-order terms are expected to reduce J_1 also in the two-orbital setting. Here, we estimate these corrections by the one-orbital prescription $t^2/U \longrightarrow t^2/U - 16t^4/U^3$. Then, e.g., for the NGO substrate, the leading contribution to $J_1^{\rm cal}$, i.e., $t_{\beta\beta}^2/(U_{\rm eff})$ with $U_{\rm eff} = U + J_H$, reduces from 47 meV to 37 meV. Applying this substitution to Eq. (1) yields the corrected exchange couplings $J_1^{\rm cal,corr}$ listed in Tab. I, which are in better agreement with the measured values (see Fig. 3).

Table I also lists the next-nearest neighbor exchange $J_2^{\rm cal}$ that can be obtained with the same second-order formula Eq. (1), except now using the hoppings t' instead of t (see Supplementary Information for details). Crucially, our calculations predict a positive J_2, in agreement with the experiment. Moreover, $J_2^{\rm cal}$ shows the same qualitative tendency as in the experiment as a function of epitaxial strain. On a quantitative level, the calculated values are, however, a factor $\sim 3-5$ lower than the experimental results. The reason is that contributions to J_2 from higher-order exchange processes, of order t^4/U^3 and $t't^2/U^2$, become (relatively) more important for $J_2^{\rm cal}$, as the second-order terms are now based on the much smaller t'.

The key difference between the *multi-orbital* case of LNO and the *one-orbital* cuprates is the larger U ($U_{cRPA} \approx 3.1$ eV for two-orbitals while $U_{cRPA} \approx 1.9$ eV for a one Ni $d_{x^2-y^2}$ orbital setup) and the additional Hund's $J_H \approx 0.5$ eV in the denominator of Eq. (1). As a consequence, the balance for the NNN exchange coupling shifts from a *ferromagnetic* ring exchange $J_2 \sim -t^4/U_{eff}^3 < 0$, that overpowers the AF second-order exchange $J_2 \sim t'^2/U_{eff} > 0$ in the one-orbital cuprates, toward dominance of the latter in the multi-orbital LNO. This change in hierarchy explains the main qualitative differences in magnon dispersion between LNO and cuprates: the opposite sign of the effective J_2. For LNO, with a positive J_2, the zone-boundary dispersion shows a notable minimum at $(1/2, 0)$, see Fig. 3, whereas a maximum occurs for the negative J_2 in cuprates.

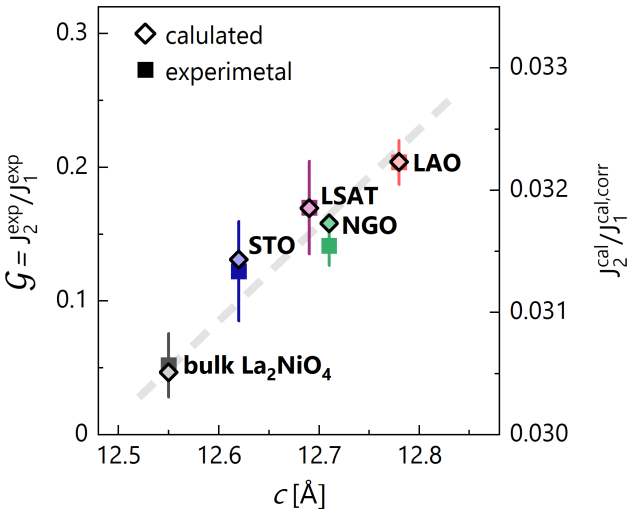

FIG. 4. **Strain dependent magnetic frustration.** The frustration parameter $\mathcal{G} = J_2^{\rm exp}/J_1^{\rm exp}$ derived from the experimental data (squares; left axis) is presented as a function of the c-axis lattice parameter. The error bars for the experimental data are calculated as a propagation of standard deviations extracted from the fits. The results for films are combined with data for bulk La_2NiO_4 from Ref. 35. The experimental frustration $\mathcal{G}$ is compared to the ratio $J_2^{\rm cal}/J_1^{\rm cal,corr}$ derived from the DFT and cRPA calculations (diamonds; right axis). Note that the calculated $J_2^{\rm cal}$ only contains a *contribution* to the full next nearest-neighbor coupling J_2. Therefore, the comparison merely highlights a similar *trend* of the frustration under in-plane compression. The dashed line is a guide-to-the-eye.

Conclusions

The *ab-initio* calculations indicate that the magnetic frustration in La_2NiO_4 is caused by the multi-orbital nature of $3d^8$ nickelates. More importantly, our results demonstrate that the degree of frustration is amplified by compressive strain (see Fig. 4), with a pivotal role played by the crystal-field splitting. Indeed, with the substrates used, the magnetic frustration increases four-fold with respect to the bulk, bridging half the way toward the exotic realm anticipated for $J_2/J_1 \sim 1/2$. Thus, our study ~~proposes~~ suggests an effective tool for tuning antiferromagnetic interactions within square lattice systems. We speculate that the approach is applicable beyond La_2NiO_4 and may offer an experimental route to reach so far unexplored regions of the magnetic phase diagram, ~~provides a design principle and experimental pathway for investigating the impact of frustration on the magnetic ground state of a J_1-J_2 square lattice, addressing a long-standing open question. It highlights that epitaxial strain can offer a powerful experimental route to reach so far unexplored regions of the magnetic phase diagram~~, potentially allowing ~~us~~ to investigate exotic states induced by magnetic frustration.

Methods

Film growth and characterization. Thin films of La_2NiO_4 were grown by RHEED-equipped Radio-frequency off-axis magnetron sputtering [55] on (001) $SrTiO_3$ (STO), (001) $LaAlO_3$ (LAO), (001) $(LaAlO_3)_{0.3}(Sr_2TaAlO_6)_{0.7}$ (LSAT) and (110) $NdGaO_3$ (NGO) substrates. These films were grown in an argon atmosphere at 700°C. Their qualities were confirmed by AFM and XRD. Their insulating character was confirmed by resistivity measurements of the LNO/STO film (see Fig. S2 in Supplementary Information).

RIXS experiments. Ni L-edge RIXS experiments for STO, LAO and NGO substrates were carried out at the I21 beamline [56] at the DIAMOND Light Source. All spectra were collected in the grazing exit geometry using linear horizontal polarized incident light with the scattering angle fixed to $2\theta = 154°$. The energy resolution was estimated from the elastic scattering on amorphous carbon tape~~,~~ and was between 37-41 meV (full-width-at-half-maximum, FWHM). All films were measured at base temperature $T = 16$ K. We define the reciprocal space (q_x, q_y, q_z) in reciprocal lattice units $(h, k, \ell) = (q_x a/2\pi, q_y b/2\pi, q_z c/2\pi)$ where a, b and c are the pseudo-tetragonal lattice parameters. RIXS spectra were acquired along three in-plane paths: $(0,0) \rightarrow (0, 1/2)$, $(0,0) \rightarrow (1/4, 1/4)$ and $(0, 1/2) \rightarrow (1/4, 1/4)$. Low-energy excitations around $(0,0)$ are limited by energy resolution. Due to kinematic constraints Γ points at higher zones cannot be reached, as well. RIXS intensities are normalized to the weight of the *dd* excitations [57]. The data for the LSAT substrate were collected at the ID32 beamline at the European Synchrotron Radiation Facility (ESRF) (see description in Supplementary Information, Fig. S3).

Phenomenological spin-wave model. The effective superexchange parameters were extracted from the measured dispersion using a linear spin wave model. We included effective couplings between the first and second nearest neighbours, plus an easy-plane anisotropy K, with the resulting Hamiltonian:

$$\mathcal{H} = J_1 \sum_{\langle i,j \rangle} \mathbf{S}_i \cdot \mathbf{S}_j + J_2 \sum_{\langle\langle i,j \rangle\rangle} \mathbf{S}_i \cdot \mathbf{S}_j + K \sum_i (S_i^z)^2 \quad (2)$$

where $\langle i,j \rangle$ and $\langle\langle i,j \rangle\rangle$ denote pairs of first and second nearest neighbours Ni atoms, respectively. The fitting procedure has been carried out using the SpinW package [58]. As an input we have used the AF structure of the bulk La_2NiO_4 determined by neutron diffraction [38–40], with the spin direction parallel to the crystallographic a-axis. The dispersion in the approximation of the linear spin wave theory is represented by [4, 35]:

$$\begin{aligned} \hbar\omega &= Z_c \sqrt{(A_{\mathbf{q}}^2 - B_{\mathbf{q}}^2)} \\ A_{\mathbf{q}} &= 4S \left[\frac{K}{4} + J_1 - J_2(1 - \nu_h \nu_k) \right] \\ B_{\mathbf{q}} &= 4S \left[J_1 \frac{\nu_h + \nu_k}{2} - \frac{K}{4} \right] \end{aligned} \quad (3)$$

where $\nu_x = \cos(2\pi x)$. The quantum renormalization factor for spin-wave velocity is fixed to $Z_c = 1.09$, as usual for $S = 1$ systems [42]. The value of the easy-plane anisotropy K mostly controls the size of the magnon gap at the Γ point. Since this value is very hard to obtain from RIXS spectra, we have fixed $K = 0.5$ meV in agreement with previous inelastic neutron scattering data [34]. We have also neglected other interactions $< 10^{-1}$ meV such as easy-axis anisotropy, inter-layer coupling and Dzyaloshinskii–Moriya interactions [35, 39].

***Ab initio* calculations.** Electronic structure calculations were performed with density functional theory in the local density approximation using a full-potential linearized muffin-tin orbital (FPLMTO) code [59], after the structures were optimized with WIEN2k [60] using the PBE functional. We mimicked the influence of the substrates by simulating bulk La_2NiO_4 using the experimental lattice constants of the thin films. The reference calculation for the bulk uses lattice constants from Ref. 35. All calculations assume the space group I4/mmm and are paramagnetic. The resulting band-structures are displayed in Fig. S4 in the Supplementary Information. The FPLMTO calculations were converged using 12^3 reducible k-points and include local orbitals for the Ni-3p and La-5p states. The internal atomic positions were relaxed with WIEN2k using 6^3 reducible k-points, a cutoff parameter RMTKMAX = 7 and partial waves inside the atomic spheres up to $l = 5$, until the forces were below 1mRy per Bohr radius (for details of the relaxed structures, see the Supplementary

Information, Table S2). The tight-binding hopping and crystal-field parameters have been extracted from a projection onto maximally localized Wannier orbitals [61, 62] of Ni $3d_{x^2-y^2}$ and $3d_{z^2}$ character. Matrix elements of the static ($\omega = 0$) and local screened Coulomb interaction (Hubbard U and Hund's J_H) have been estimated from calculations in the constrained random phase approximation (cRPA) [53] for entangled band-structures [63] in the Wannier basis [62] using $6 \times 6 \times 6$ reducible momentum-points in the Brillouin zone. For the two-particle product basis, states are kept up to an angular cutoff of $l = 4$ and down to an overlap eigenvalue of 10^{-4}.

Data availability

~~The data that support~~ Data supporting the findings of this study are available from the corresponding author upon reasonable request.

Author contributions

I.B. and L.M. have contributed equally to this work. G.D.L., C.B.E., A.D., L.G., A.E., S.J. and M.G. grew and characterized the La_2NiO_4 films. I.B., J.Choi, M.G-F., S.A., K-J.Z, K.K., N.B.B. and Q.W. carried out the RIXS experiments. I.B., L.M. and Q.W. analysed the RIXS data. P.M., J.M.T and K.H. conceived, executed and analysed the *ab initio* calculations. I.B., Q.W. and J.C. conceived the project. All authors contributed to the writing of the manuscript.

Acknowledgements

I.B. and L.M. acknowledge support from the Swiss Government Excellence Scholarship under project numbers ESKAS-Nr: 2022.0001 and ESKAS-Nr: 2023.0052. G.D.L, M.G. and J.C. thank the Swiss National Science Foundation under Projects No. 200021_188564 and PP00P2_170564. Q.W. is supported by the Research Grants Council of Hong Kong (ECS No. 24306223), and the CUHK Direct Grant (No. 4053613). G.D.L. acknowledges support from the UZH GRC Travel Grant. We acknowledge Diamond Light Source for providing beam time on beamline I21 under Proposal MM30189 and the European Synchrotron Radiation Facility (ESRF) for providing beam time on beamline ID32 under Proposal HC 5241. C.B.E. acknowledges support for this research through a Vannevar Bush Faculty Fellowship (ONR N00014-20-1-2844), the Gordon and Betty Moore Foundation's EPiQS Initiative, Grant GBMF9065 and NSF through the University of Wisconsin Materials Research Science and Engineering Center (DMR-2309000). The synthesis of thin films at the University of Wisconsin-Madison was supported by the US Department of Energy (DOE), Office of Science, Office of Basic Energy Sciences (BES), under award number DE-FG02-06ER46327.

Competing interests

The authors declare that they have no competing interests.

[1] P. A. Lee, N. Nagaosa, and X.-G. Wen, Doping a Mott insulator: Physics of high-temperature superconductivity, Rev. Mod. Phys. **78**, 17 (2006).
[2] N. B. Christensen, H. M. Rønnow, D. F. McMorrow, A. Harrison, T. G. Perring, M. Enderle, R. Coldea, L. P. Regnault, and G. Aeppli, Quantum dynamics and entanglement of spins on a square lattice, PNAS **104**, 15264 (2007).
[3] N. S. Headings, S. M. Hayden, R. Coldea, and T. G. Perring, Anomalous High-Energy Spin Excitations in the High-T_c Superconductor-Parent Antiferromagnet La_2CuO_4, Phys. Rev. Lett. **105**, 247001 (2010).
[4] R. Coldea, S. M. Hayden, G. Aeppli, T. G. Perring, C. D. Frost, T. E. Mason, S.-W. Cheong, and Z. Fisk, Spin waves and electronic interactions in La_2CuO_4, Phys. Rev. Lett. **86**, 5377 (2001).
[5] Q. Wang, S. Mustafi, E. Fogh, N. Astrakhantsev, Z. He, I. Biało, M. Horio, O. Ivashko, N. E. Shaik, K. von Arx, Y. Sassa, E. Paris, M. H. Fischer, Y. Tseng, N. B. Christensen, A. Galdi, D. G. Schlom, K. M. Shen, T. Schmitt, H. M. Rønnow, and J. Chang, Quantum fluctuations in a weakly correlated Mott insulator, arXiv:2311.16553 (2023).
[6] K. Choo, T. Neupert, and G. Carleo, Two-dimensional frustrated J_1-J_2 model studied with neural network quantum states, Phys. Rev. B **100**, 125124 (2019).
[7] L. Capriotti and S. Sorella, Spontaneous plaquette dimerization in the $J_1 - J_2$ Heisenberg model, Phys. Rev. Lett. **84**, 3173 (2000).
[8] L. Capriotti, F. Becca, A. Parola, and S. Sorella, Resonating valence bond wave functions for strongly frustrated spin systems, Phys. Rev. Lett. **87**, 097201 (2001).
[9] G.-M. Zhang, H. Hu, and L. Yu, Valence-bond spin-liquid state in two-dimensional frustrated spin-1/2 Heisenberg antiferromagnets, Phys. Rev. Lett. **91**, 067201 (2003).
[10] S.-S. Gong, W. Zhu, D. N. Sheng, O. I. Motrunich, and M. P. A. Fisher, Plaquette ordered phase and quantum phase diagram in the spin-$\frac{1}{2}$ J_1-J_2 square Heisenberg model, Phys. Rev. Lett. **113**, 027201 (2014).
[11] O. P. Sushkov, J. Oitmaa, and Z. Weihong, Quantum phase transitions in the two-dimensional J_1-J_2 model, Phys. Rev. B **63**, 104420 (2001).
[12] H. C. Jiang, F. Krüger, J. E. Moore, D. N. Sheng, J. Zaanen, and Z. Y. Weng, Phase diagram of the frustrated spatially-anisotropic $S = 1$ antiferromagnet on a square lattice, Phys. Rev. B **79**, 174409 (2009).
[13] P. W. Anderson, The Resonating Valence Bond State in La_2CuO_4 and Superconductivity, Science **235**, 1196 (1987).
[14] E. Dagotto and A. Moreo, Phase diagram of the frustrated spin-1/2 Heisenberg antiferromagnet in 2 dimensions, Phys. Rev. Lett. **63**, 2148 (1989).

[15] H. J. Schulz, T. A. Ziman, and D. Poilblanc, Magnetic order and disorder in the frustrated quantum Heisenberg antiferromagnet in two dimensions, Journal de Physique I **6**, 675–703 (1996).

[16] K. S. D. Beach, Master equation approach to computing RVB bond amplitudes, Phys. Rev. B **79**, 224431 (2009).

[17] Q. Wang, Y. Shen, B. Pan, X. Zhang, K. Ikeuchi, K. Iida, A. D. Christianson, H. C. Walker, D. T. Adroja, M. Abdel-Hafiez, X. Chen, D. A. Chareev, A. N. Vasiliev, and J. Zhao, Magnetic ground state of FeSe, Nat. Commun. **7**, 12182 (2016).

[18] Y. Gu, Q. Wang, H. Wo, Z. He, H. C. Walker, J. T. Park, M. Enderle, A. D. Christianson, W. Wang, and J. Zhao, Frustrated magnetic interactions in FeSe, Phys. Rev. B **106**, L060504 (2022).

[19] O. Mustonen, S. Vasala, E. Sadrollahi, K. P. Schmidt, C. Baines, H. C. Walker, I. Terasaki, F. J. Litterst, E. Baggio-Saitovitch, and M. Karppinen, Spin-liquid-like state in a spin-1/2 square-lattice antiferromagnet perovskite induced by $d^{10}-d^0$ cation mixing, Nat. Commun. **9**, 1085 (2018).

[20] O. Ivashko, M. Horio, W. Wan, N. B. Christensen, D. E. McNally, E. Paris, Y. Tseng, N. E. Shaik, H. M. Rønnow, H. I. Wei, C. Adamo, C. Lichtensteiger, M. Gibert, M. R. Beasley, K. M. Shen, J. M. Tomczak, T. Schmitt, and J. Chang, Strain-engineering Mott-insulating La_2CuO_4, Nat. Commun. **10**, 786 (2019).

[21] J. Goodenough and S. Ramasesha, Further evidence for the coexistence of localized and itinerant 3*d* electrons in La_2NiO_4, Materials Research Bulletin **17**, 383 (1982).

[22] P. G. Radaelli, D. G. Hinks, A. W. Mitchell, B. A. Hunter, J. L. Wagner, B. Dabrowski, K. G. Vandervoort, H. K. Viswanathan, and J. D. Jorgensen, Structural and superconducting properties of $La_{2-x}Sr_xCuO_4$ as a function of Sr content, Phys. Rev. B **49**, 4163 (1994).

[23] A. Nag, H. C. Robarts, F. Wenzel, J. Li, H. Elnaggar, R.-P. Wang, A. C. Walters, M. García-Fernández, F. M. F. de Groot, M. W. Haverkort, and K.-J. Zhou, Many-body physics of single and double spin-flip excitations in NiO, Phys. Rev. Lett. **124**, 067202 (2020).

[24] G. Ghiringhelli, M. Matsubara, C. Dallera, F. Fracassi, R. Gusmeroli, A. Piazzalunga, A. Tagliaferri, N. B. Brookes, A. Kotani, and L. Braicovich, NiO as a test case for high resolution resonant inelastic soft x-ray scattering, J. Phys.: Condens. Matter **17**, 5397 (2005).

[25] J. Q. Lin, P. Villar Arribi, G. Fabbris, A. S. Botana, D. Meyers, H. Miao, Y. Shen, D. G. Mazzone, J. Feng, S. G. Chiuzbăian, A. Nag, A. C. Walters, M. García-Fernández, K.-J. Zhou, J. Pelliciari, I. Jarrige, J. W. Freeland, J. Zhang, J. F. Mitchell, V. Bisogni, X. Liu, M. R. Norman, and M. P. M. Dean, Strong superexchange in a $d^{9-\delta}$ nickelate revealed by resonant inelastic x-ray scattering, Phys. Rev. Lett. **126**, 087001 (2021).

[26] P. Kuiper, J. van Elp, D. E. Rice, D. J. Buttrey, H.-J. Lin, and C. T. Chen, Polarization-dependent nickel 2*p* x-ray-absorption spectra of $La_2NiO_{4+\delta}$, Phys. Rev. B **57**, 1552 (1998).

[27] G. Ghiringhelli, A. Piazzalunga, C. Dallera, T. Schmitt, V. N. Strocov, J. Schlappa, L. Patthey, X. Wang, H. Berger, and M. Grioni, Observation of Two Nondispersive Magnetic Excitations in NiO by Resonant Inelastic Soft-X-Ray Scattering, Phys. Rev. Lett. **102**, 027401 (2009).

[28] L. J. P. Ament, M. van Veenendaal, T. P. Devereaux, J. P. Hill, and J. van den Brink, Resonant inelastic x-ray scattering studies of elementary excitations, Rev. Mod. Phys. **83**, 705 (2011).

[29] L. Martinelli, D. Betto, K. Kummer, R. Arpaia, L. Braicovich, D. Di Castro, N. B. Brookes, M. Moretti Sala, and G. Ghiringhelli, Fractional Spin Excitations in the Infinite-Layer Cuprate $CaCuO_2$, Phys. Rev. X **12**, 021041 (2022).

[30] Q. Wang, K. von Arx, M. Horio, D. J. Mukkattukavil, J. Küspert, Y. Sassa, T. Schmitt, A. Nag, S. Pyon, T. Takayama, H. Takagi, M. Garcia-Fernandez, K.-J. Zhou, and J. Chang, Charge order lock-in by electron-phonon coupling in $La_{1.675}Eu_{0.2}Sr_{0.125}CuO_4$, Sci. Adv. **7**, eabg7394 (2021).

[31] L. Pintschovius, J. M. Bassat, P. Odier, F. Gervais, G. Chevrier, W. Reichardt, and F. Gompf, Lattice dynamics of La_2NiO_4, Phys. Rev. B **40**, 2229 (1989).

[32] L. Pintschovius, J.-M. Bassat, P. Odier, F. Gervais, B. Hennion, and W. Reichardt, Phonon Anomalies in La_2NiO_4, Europhysics Letters **5**, 247 (1988).

[33] G. Fabbris, D. Meyers, L. Xu, V. M. Katukuri, L. Hozoi, X. Liu, Z.-Y. Chen, J. Okamoto, T. Schmitt, A. Uldry, B. Delley, G. D. Gu, D. Prabhakaran, A. T. Boothroyd, J. van den Brink, D. J. Huang, and M. P. M. Dean, Doping Dependence of Collective Spin and Orbital Excitations in the Spin-1 Quantum Antiferromagnet $La_{2-x}Sr_xNiO_4$ Observed by X Rays, Phys. Rev. Lett. **118**, 156402 (2017).

[34] K. Nakajima, K. Yamada, S. Hosoya, T. Omata, and Y. Endoh, Spin-Wave Excitations in Two Dimensional Antiferromagnet of Stoichiometric La_2NiO_4, Journal of the Physical Society of Japan **62**, 4438–4448 (1993).

[35] A. N. Petsch, N. S. Headings, D. Prabhakaran, A. I. Kolesnikov, C. D. Frost, A. T. Boothroyd, R. Coldea, and S. M. Hayden, High-energy spin waves in the spin-1 square-lattice antiferromagnet La_2NiO_4, Phys. Rev. Res. **5**, 033113 (2023).

[36] Y. Y. Peng, G. Dellea, M. Minola, M. Conni, A. Amorese, D. Di Castro, G. M. De Luca, K. Kummer, M. Salluzzo, X. Sun, X. J. Zhou, G. Balestrino, M. Le Tacon, B. Keimer, L. Braicovich, N. B. Brookes, and G. Ghiringhelli, Influence of apical oxygen on the extent of in-plane exchange interaction in cuprate superconductors, Nature Phys. **13**, 1201–1206 (2017).

[37] O. Ivashko, N. E. Shaik, X. Lu, C. G. Fatuzzo, M. Dantz, P. G. Freeman, D. E. McNally, D. Destraz, N. B. Christensen, T. Kurosawa, N. Momono, M. Oda, C. E. Matt, C. Monney, H. M. Rønnow, T. Schmitt, and J. Chang, Damped spin excitations in a doped cuprate superconductor with orbital hybridization, Phys. Rev. B **95**, 214508 (2017).

[38] G. Aeppli and D. J. Buttrey, Magnetic Correlations in $La_2NiO_{4+\delta}$, Phys. Rev. Lett. **61**, 203 (1988).

[39] K. Yamada, T. Omata, K. Nakajima, S. Hosoya, T. Sumida, and Y. Endoh, Magnetic structure and weak ferromagnetism of $La_2NiO_{4+\delta}$, Physica C: Superconductivity **191**, 15 (1992).

[40] J. Rodriguez-Carvajal, M. T. Fernandez-Diaz, and J. L. Martinez, Neutron diffraction study on structural and magnetic properties of La_2NiO_4, J. Phys.: Condens. Matter **3**, 3215 (1991).

[41] K. Yamada, M. Arai, Y. Endoh, S. Hosoya, K. Nakajima, T. Perring, and A. Taylor, Complete Two-Dimensional Antiferromagnetic Spin-Wave Dispersion Relation of

La_2NiO_4 Determined by Chopper Spectrometer Installed at the Pulsed Neutron Source, J. Phys. Soc. Jpn. **60**, 1197 (1991).

[42] J. Igarashi, $1/S$ expansion for thermodynamic quantities in a two-dimensional Heisenberg antiferromagnet at zero temperature, Phys. Rev. B **46**, 10763 (1992).

[43] H. Lu, M. Rossi, A. Nag, M. Osada, D. F. Li, K. Lee, B. Y. Wang, M. Garcia-Fernandez, S. Agrestini, Z. X. Shen, E. M. Been, B. Moritz, T. P. Devereaux, J. Zaanen, H. Y. Hwang, K.-J. Zhou, and W. S. Lee, Magnetic excitations in infinite-layer nickelates, Science **373**, 213 (2021).

[44] Q. Gao, S. Fan, Q. Wang, J. Li, X. Ren, I. Biało, A. Drewanowski, P. Rothenbühler, J. Choi, Y. Wang, T. Xiang, J. Hu, K.-J. Zhou, V. Bisogni, R. Comin, J. Chang, J. Pelliciari, X. J. Zhou, and Z. Zhu, Magnetic Excitations in Strained Infinite-layer Nickelate $PrNiO_2$, arXiv:2208.05614 (2022).

[45] J.-Y. P. Delannoy, M. J. P. Gingras, P. C. W. Holdsworth, and A.-M. S. Tremblay, Low-energy theory of the $t - t^{'} - t^{''} - U$ Hubbard model at half-filling: Interaction strengths in cuprate superconductors and an effective spin-only description of La_2CuO_4, Phys. Rev. B **79**, 235130 (2009).

[46] B. Dalla Piazza, M. Mourigal, M. Guarise, H. Berger, T. Schmitt, K. J. Zhou, M. Grioni, and H. M. Rønnow, Unified one-band hubbard model for magnetic and electronic spectra of the parent compounds of cuprate superconductors, Phys. Rev. B **85**, 100508 (2012).

[47] M. Horio, C. E. Matt, K. Kramer, D. Sutter, A. M. Cook, Y. Sassa, K. Hauser, M. Månsson, N. C. Plumb, M. Shi, O. J. Lipscombe, S. M. Hayden, T. Neupert, and J. Chang, Two-dimensional type-II Dirac fermions in layered oxides, Nat. Commun. **9**, 3252 (2018).

[48] M. Uchida, K. Ishizaka, P. Hansmann, X. Yang, M. Sakano, J. Miyawaki, R. Arita, Y. Kaneko, Y. Takata, M. Oura, A. Toschi, K. Held, A. Chainani, O. K. Andersen, S. Shin, and Y. Tokura, Orbital characters of three-dimensional Fermi surfaces in $Eu_{2-x}Sr_xNiO_4$ as probed by soft-x-ray angle-resolved photoemission spectroscopy, Phys. Rev. B **84**, 241109 (2011).

[49] M. Uchida, K. Ishizaka, P. Hansmann, Y. Kaneko, Y. Ishida, X. Yang, R. Kumai, A. Toschi, Y. Onose, R. Arita, K. Held, O. K. Andersen, S. Shin, and Y. Tokura, Pseudogap of Metallic Layered Nickelate $R_{2-x}Sr_xNiO_4$ (R = Nd, Eu) Crystals Measured Using Angle-Resolved Photoemission Spectroscopy, Phys. Rev. Lett. **106**, 027001 (2011).

[50] C. E. Matt, D. Sutter, A. M. Cook, Y. Sassa, M. Månsson, O. Tjernberg, L. Das, M. Horio, D. Destraz, C. G. Fatuzzo, K. Hauser, M. Shi, M. Kobayashi, V. N. Strocov, T. Schmitt, P. Dudin, M. Hoesch, S. Pyon, T. Takayama, H. Takagi, O. J. Lipscombe, S. M. Hayden, T. Kurosawa, N. Momono, M. Oda, T. Neupert, and J. Chang, Direct observation of orbital hybridisation in a cuprate superconductor, Nat. Commun. **9**, 972 (2018).

[51] J. M. Tomczak, T. Miyake, R. Sakuma, and F. Aryasetiawan, Effective Coulomb interactions in solids under pressure, Phys. Rev. B **79**, 235133 (2009).

[52] R. Lemanski and J. Matysiak, Two-orbital Hubbard model vs spin S = 1 Heisenberg model: Studies on clusters, Condensed Matter Physics **21**, 33301 (2018).

[53] F. Aryasetiawan, M. Imada, A. Georges, G. Kotliar, S. Biermann, and A. I. Lichtenstein, Frequency-dependent local interactions and low-energy effective models from electronic structure calculations, Phys. Rev. B **70**, 195104 (2004).

[54] A. H. MacDonald, S. M. Girvin, and D. Yoshioka, Reply to "Comment on 't/U expansion for the Hubbard model"', Phys. Rev. B **41**, 2565 (1990).

[55] J. P. Podkaminer, J. J. Patzner, B. A. Davidson, and C. B. Eom, Real-time and *in situ* monitoring of sputter deposition with RHEED for atomic layer controlled growth, APL Materials **4**, 086111 (2016).

[56] K.-J. Zhou, A. Walters, M. Garcia-Fernandez, T. Rice, M. Hand, A. Nag, J. Li, S. Agrestini, P. Garland, H. Wang, S. Alcock, I. Nistea, B. Nutter, N. Rubies, G. Knap, M. Gaughran, F. Yuan, P. Chang, J. Emmins, and G. Howell, I21: an advanced high-resolution resonant inelastic X-ray scattering beamline at Diamond Light Source, J. Synchrotron Rad. **29**, 563 (2022).

[57] Q. Wang, M. Horio, K. von Arx, Y. Shen, D. John Mukkattukavil, Y. Sassa, O. Ivashko, C. E. Matt, S. Pyon, T. Takayama, H. Takagi, T. Kurosawa, N. Momono, M. Oda, T. Adachi, S. M. Haidar, Y. Koike, Y. Tseng, W. Zhang, J. Zhao, K. Kummer, M. Garcia-Fernandez, K.-J. Zhou, N. B. Christensen, H. M. Rønnow, T. Schmitt, and J. Chang, High-temperature charge-stripe correlations in $La_{1.675}Eu_{0.2}Sr_{0.125}CuO_4$, Phys. Rev. Lett. **124**, 187002 (2020).

[58] S. Toth and B. Lake, Linear spin wave theory for single-Q incommensurate magnetic structures, Journal of Physics: Condensed Matter **27**, 166002 (2015).

[59] M. Methfessel, M. van Schilfgaarde, and R. Casali, A full-potential lmto method based on smooth hankel functions, in Electronic Structure and Physical Properties of Solids: The Uses of the LMTO Method, Lecture Notes in Physics. H. Dreysse, ed. **535** (2000).

[60] P. Blaha, K. Schwarz, F. Tran, R. Laskowski, G. K. H. Madsen, and L. D. Marks, WIEN2k: An APW+lo program for calculating the properties of solids, J. Chem. Phys. **152**, 074101 (2020).

[61] N. Marzari, A. A. Mostofi, J. R. Yates, I. Souza, and D. Vanderbilt, Maximally localized Wannier functions: Theory and applications, Rev. Mod. Phys. **84**, 1419 (2012).

[62] T. Miyake and F. Aryasetiawan, Screened Coulomb interaction in the maximally localized Wannier basis, Phys. Rev. B **77**, 085122 (2008).

[63] T. Miyake, F. Aryasetiawan, and M. Imada, *Ab initio* procedure for constructing effective models of correlated materials with entangled band structure, Phys. Rev. B **80**, 155134 (2009).